

# Probing substrate-dependent long-range surface structure of single-layer and multilayer MoS<sub>2</sub> by low-energy electron microscopy and microprobe diffraction

Po-Chun Yeh,<sup>1</sup> Wencan Jin,<sup>2</sup> Nader Zaki,<sup>1</sup> Datong Zhang,<sup>2</sup> Jerzy T. Sadowski,<sup>3</sup> Abdullah Al-Mahboob,<sup>3</sup> Arend M. van der Zande,<sup>4,5</sup> Daniel A. Chenet,<sup>5</sup> Jerry I. Dadap,<sup>2</sup> Irving P. Herman,<sup>2</sup> Peter Sutter,<sup>3</sup> James Hone,<sup>5</sup> and Richard M. Osgood, Jr.<sup>1,2</sup>

<sup>1</sup>*Department of Applied Physics and Applied Mathematics, Columbia University, New York, New York 10027, USA*

<sup>2</sup>*Department of Electrical Engineering, Columbia University, New York, New York 10027, USA*

<sup>3</sup>*Center for Functional Nanomaterials, Brookhaven National Laboratory, Upton, New York 11973, USA*

<sup>4</sup>*Energy Frontier Research Center, Columbia University, New York, New York 10027, USA*

<sup>5</sup>*Department of Mechanical Engineering, Columbia University, New York, New York 10027, USA*

(Received 17 December 2013; revised manuscript received 14 February 2014; published 4 April 2014)

The long-range surface structure of the dichalcogenide MoS<sub>2</sub> is probed with nanometer-length spatial resolution using low-energy electron microscopy (LEEM) and microprobe low-energy electron diffraction ( $\mu$ -LEED). The quality of two differently prepared types of MoS<sub>2</sub>, single-layer and multilayer exfoliated crystals, as well as single-layer chemical-vapor-deposition (CVD)-grown crystals, is examined. The effects induced by a supporting interface are examined by utilizing two different substrates, SiO<sub>2</sub> and native-oxide-covered Si. In addition, the role of impurities is also studied by way of *in situ* deposition of the alkali-metal potassium. Microprobe measurements reveal that, unlike exfoliated MoS<sub>2</sub>, CVD-grown MoS<sub>2</sub> may, in some instances, exhibit large-scale grain-boundary alterations due to the presence of surface strain during growth. However, real-space probing by LEEM in conjunction with *k*-space probing by  $\mu$ -LEED shows that the quality of CVD-grown MoS<sub>2</sub> can be comparable to that of exfoliated MoS<sub>2</sub>.

DOI: [10.1103/PhysRevB.89.155408](https://doi.org/10.1103/PhysRevB.89.155408)

PACS number(s): 61.05.jh, 68.37.Nq, 68.55.-a

## I. INTRODUCTION

Single-layer MoS<sub>2</sub> is a metal dichalcogenide two-dimensional crystal that has emerged as a representative of a new class of materials with distinctive physical [1], electronic [2–6], and optical [7–11] properties. Due to its semiconducting [7,12] nature and large intrinsic optical direct band gap of 1.8 eV [12], monolayer (ML) MoS<sub>2</sub> is ideal for potential applications in nano-optoelectronics and energy harvesting. Recent studies in controlling dynamic valley-spin polarization in ML MoS<sub>2</sub> films [8–10] also suggest initial exploration of spintronic applications. Finally, various forms of MoS<sub>2</sub> such as nanotubes [13], nanoparticles [14], and monolayer films [15,16] have been explored. However, while extensive research has been performed on preparation of carbon-based materials, including monolayer graphene, studies on the crystal growth of monolayer MoS<sub>2</sub> are relatively sparse. Among the existing studies, it has been demonstrated that polycrystalline monolayer MoS<sub>2</sub> can be grown via solid-source chemical vapor deposition (CVD) [17–22], allowing its use in thin-film microdevice applications. Recently, the Hone Group and their collaborators have shown that it is possible to grow high-quality, ML-thick crystals of MoS<sub>2</sub> with typical sizes of a few hundreds of micrometers, which have optical and transport properties comparable to those of exfoliated MoS<sub>2</sub> [21]. In short, these developments suggest single-layer MoS<sub>2</sub>, including now CVD-grown material, as an ideal candidate for building atomically thin-layered electronic [23–25], optical [12,26], and photovoltaic [27] devices.

Despite the promise of this relatively available two-dimensional (2D) material, its characterization has been generally limited to optical and transport probes. Furthermore, the almost exclusive use of a thick oxide as the supporting substrate has been important in order to allow optical

microscopic characterization of the 2D material. Hence, to the best of our knowledge, this has prohibited studies of this material on other surfaces, and it has precluded the discovery of potentially rich interface interactions that may exist between a 2D dichalcogenide, such as MoS<sub>2</sub>, and its supporting substrate. In order to study monolayer MoS<sub>2</sub> on other substrates other than thick oxides, it would be ideal for an investigative technique to possess the following three imaging modalities: (1) real-space microscopy, which would allow locating of MoS<sub>2</sub> samples, (2) spatially resolved diffraction, which would allow confirmation of crystalline quality and domain orientation of MoS<sub>2</sub> samples, and (3), spatially resolved spectroscopy, which would allow electronic structure mapping of MoS<sub>2</sub> samples. In this paper, we use electron microprobes in an ultrahigh-vacuum (UHV) environment to achieve the first two desired imaging modalities on MoS<sub>2</sub> and discuss new insights into MoS<sub>2</sub> materials that are afforded by this technique.

Specifically, this study has characterized and probed mono- and multilayer exfoliated MoS<sub>2</sub> and monolayer CVD-grown MoS<sub>2</sub> using a high-resolution direct imaging instrument: viz. a spectroscopic photoemission and low-energy electron microscope (SPE-LEEM) [27,28], which is capable of carrying out structural and spectroscopic analysis of the sample at the nanometer scale [29–31]. Our studies provide information about the surface corrugation and crystalline structure of the ultrathin films under investigation. Our measurements were carried out on two different substrates: thermally oxidized 285-nm-thick SiO<sub>2</sub>/Si wafers and a Si wafer with a thin native SiO<sub>2</sub> film. Our results complement earlier optical studies done using Raman and photoluminescence measurements [7,12,17–21]. Furthermore, in order to tune the Fermi level and/or work function of MoS<sub>2</sub> via surface doping [32,33], we have used atomic potassium dosing. Note that this doping is done *in situ*,

thus allowing the surface morphology and structure to be examined by LEEM and microprobe low-energy electron diffraction ( $\mu$ -LEED) in the presence or absence of doping. A comparative analysis of the results obtained from MoS<sub>2</sub> samples fabricated with different methods and on different substrates provides understanding of the properties and qualities of CVD-grown MoS<sub>2</sub> and sheds light on potential applications of monolayer CVD MoS<sub>2</sub> for improved electronic and optical devices, and on two-dimensional conjoined materials, such as heterojunctions with graphene [25,34,35] and other 2D materials.

## II. EXPERIMENTAL METHODS

The samples examined here were either mechanically exfoliated or prepared by CVD growth on a high-quality SiO<sub>2</sub>/Si substrate, as first described in Ref. [21], and they were examined on the growth substrate or transferred onto Si substrates, with thermally grown or native-oxide overlayers, using sacrificial polymer layers [36]. The samples were then annealed at 350 °C under a laminar flow of N<sub>2</sub>/Ar to complete the transfer procedure. Prior to SPE-LEEM experiments, the samples were degassed at 350 °C for several hours under UHV conditions. In certain experiments, the samples were surface-doped with different levels of potassium while in the LEEM chamber (see below).

## III. EXPERIMENT RESULTS

### A. Calibration experiments on exfoliated MoS<sub>2</sub>

#### 1. LEEM on SiO<sub>2</sub>-supported exfoliated MoS<sub>2</sub>

LEEM measurements were first carried out on mechanically exfoliated MoS<sub>2</sub> flakes prepared *ex situ* on a silicon wafer with a 285-nm-thick SiO<sub>2</sub> overlayer. Since LEEM imposes a relatively large incident electron flux of  $5 \times 10^8 \text{ sec}^{-1} \mu\text{m}^{-2}$  onto samples with areas of 20–50  $\mu\text{m}^2$ , preventing or reducing charging of the sample was necessary to perform LEEM measurements. The low mobility of ML dichalcogenide systems, especially MoS<sub>2</sub> [37,38], makes this charging issue even more severe. Thus developing a strategy for eliminating charging was a major experimental necessity. Our initial approach was to bring MoS<sub>2</sub> islands into contact with a uniform-potential metallic plane by employing Au grids, which were in electrical contact with the local instrument “ground.” This approach was realized by using transmission electron microscopy (TEM) grids as shadow masks to create thermally evaporated Au/Cr/Al, 40/5/10-nm-thick, metal contacts on MoS<sub>2</sub> islands, as shown in Figs. 1(a) and 1(b). Note that in Fig. 1(b), the profile of the MoS<sub>2</sub> sample buried under the contacts can be clearly seen via reflectivity differences between the contacts and the MoS<sub>2</sub> in this LEEM image. Despite this “grounding” grid, local charging of the sample effectively prevented LEEM under continuous electron beam illumination. The very low mobility of MoS<sub>2</sub> ( $< 10 \text{ cm}^2/\text{V}\cdot\text{s}$ ) [37] prevents compensation of the charge that accumulates in the thick SiO<sub>2</sub> when it is irradiated with electrons in LEEM. In other words, the flux of incoming charges is much larger than the outgoing flux, which is conducted to ground by metal contacts. Charging was present over a wide range of grid spacings (5–30  $\mu\text{m}$ ) and contact thickness (5–100 nm). For the example of the MoS<sub>2</sub> sample in Fig. 1(b), which consists of 1 ML and 2 ML regions,

the boundaries between the two regions, as well as the edges of the MoS<sub>2</sub> sample in contact with the metal, became blurry after extended ( $> 5$  min) exposure to the LEEM electron beam. In an attempt to inhibit charging, potassium deposition was tried; however, this proved ineffective. Note, however, that in the case of  $\mu$ -LEED measurements, the incident electron energy was much higher (20–100 eV) than in the case of LEEM. This higher energy range led to a reduction in surface charging due, in part, to a higher secondary electron yield, which helped to balance the incident electron flux. Thus, in this case, it was found that a Au grid was then sufficient to satisfactorily reduce any charge-induced distortion of the LEED pattern.

By using a short-duration (3–5 min) LEEM electron exposure before the full onset of charging, measurements of a metal-grid-covered MoS<sub>2</sub> surface were possible. These measurements showed a relatively defect-free surface structure, as compared to the speckled appearance of graphene on SiO<sub>2</sub> [39]. In Fig. 1(b), the LEEM measurement shows that the image distortion happens mostly on the borders of MoS<sub>2</sub>, with SiO<sub>2</sub> and with Au, as a result of charge accumulation. This gives an idea of charge-transfer dynamics in insulator/dichalcogenide and metal/dichalcogenide systems, and it opens the possibility of studying it more extensively using a derivative of this technique.

#### 2. LEEM on Si-supported exfoliated MoS<sub>2</sub>

In order to improve the quality of our LEEM measurements, an alternate approach was used, namely, transfer of the sample to a Si substrate covered only by a native-oxide layer. A similar approach has been reported previously for imaging ML-thick organic materials of low mobility, i.e., using a conductive substrate so as to provide a large-area channel for charge dissipation [40] in an effort to balance the huge incoming flux of charge from LEEM. The transfer process is illustrated in Fig. 1(c). While use of this native-oxide-covered substrate entailed a more complex sample preparation procedure, tunneling through this thin oxide from the MoS<sub>2</sub> sample was found to be effective in preventing charging. However, the thin native oxide, typically of  $\sim 10 \text{ \AA}$  thickness, was too thin to allow sufficient optical contrast for easy optical examination of the MoS<sub>2</sub> thin films. Thus, a Si sample with a standard 300-nm-thickness-oxide overlayer was used for exfoliation and initial sample handling, followed by transfer of the MoS<sub>2</sub> to a separate native-oxide-covered Si substrate for LEEM imaging of the sample. Figures 1(d) and 1(e) shows examples of optical and LEEM images of a MoS<sub>2</sub> flake before and after transfer, respectively. It is clear from the sharp image resolution that this approach prevented significant charging of the MoS<sub>2</sub> flake. In addition, LEEM imaging was relatively uniform across the surface, except near the flake edges. In our LEEM imaging, the electron energies were chosen to obtain good contrast between laterally adjacent MoS<sub>2</sub> samples of different thicknesses. Note that removal of electronic detector-screen artifacts and background signal, by background subtraction of a scaled background image, also improved the image contrast, as shown in Fig. 1(f). Finally, as in the SiO<sub>2</sub>-substrate-supported case, LEEM measurements of MoS<sub>2</sub> were performed after deposition of potassium; see Fig. 1(g). The figure clearly shows that the quality of LEEM images and layer contrast

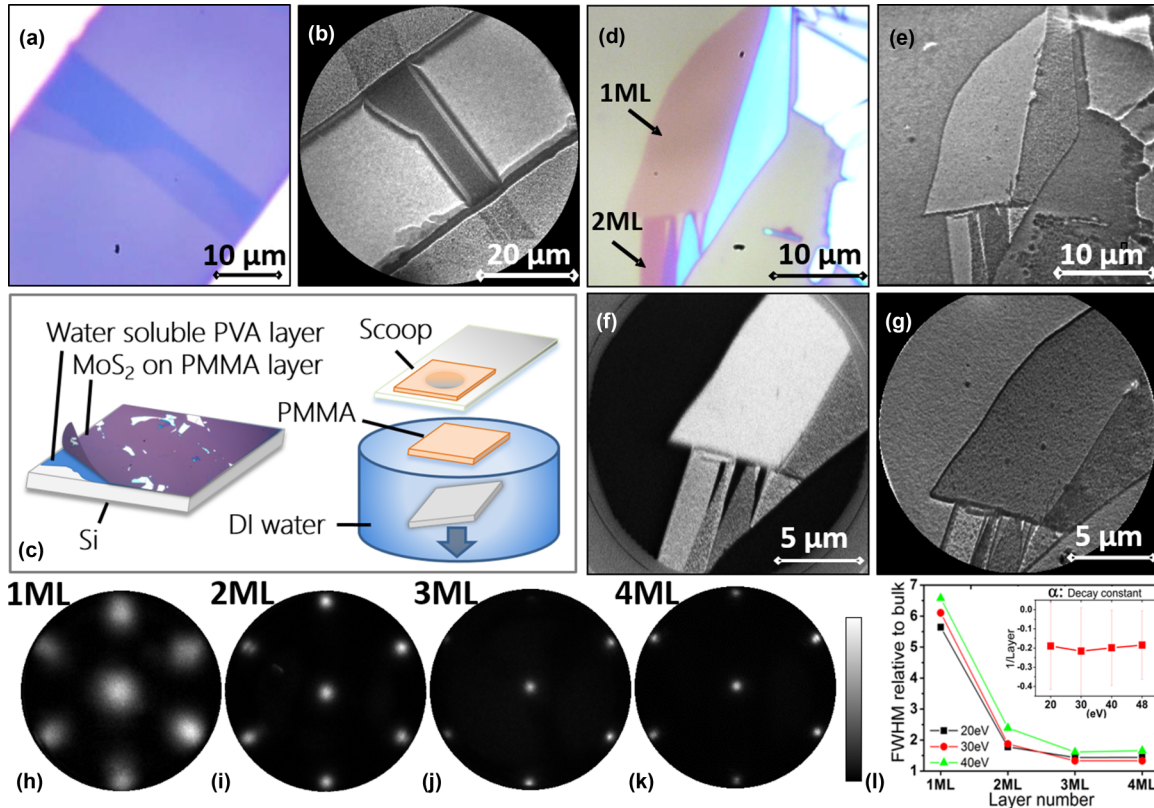


FIG. 1. (Color online) Exfoliated MoS<sub>2</sub> on SiO<sub>2</sub> and Si. (a) Optical microscope image of an exfoliated 1–2 ML MoS<sub>2</sub> flake on SiO<sub>2</sub>, with both its top and bottom side contacted. The bright areas correspond to Au/Cr/Al contacts. (b) LEEM image of the same sample. At an electron energy of 0.9 eV, the MoS<sub>2</sub> beneath the metal contacts can be clearly seen. (c) Illustration of the transfer process of exfoliated MoS<sub>2</sub>. The polymethyl methacrylate (PMMA) film with bonded MoS<sub>2</sub> flakes is “scooped up” and stamped on a substrate of interest. (d) Optical microscope image of an exfoliated mixed-layer flake on SiO<sub>2</sub>, before transfer; and (e) after transfer to Si and probed by MEM imaging (0.08 eV). (f) LEEM image (5 eV) after removal of background signal; (g) MEM image (0.08 eV) after K doping. (h)–(k)  $\mu$ -LEED patterns at 48 eV electron energy on exfoliated 1–4 ML MoS<sub>2</sub>, post-transfer to Si. For samples with thicknesses > 1 ML, the LEED signal quality is akin to that of a bulk crystal. Also, the LEED (00) spot width decreases with increasing layer number. (l) FWHM of the (00) LEED spot for 1–4 ML MoS<sub>2</sub> flakes relative to that of bulk, measured at 20, 30, and 40 eV. The inset shows the extracted decay rate of the FWHM with increasing layer number as a function of electron energy.

were improved by the presence of potassium, and as expected, an overall lowering of the work function also occurred. Note that the changes in local work function can be calibrated and measured by mirror electron microscopy (MEM) [41–43] via changes in the electron reflectivity [44–46].

Thus, our results show that a doped Si substrate, even in the presence of a native oxide, can ground typical MoS<sub>2</sub> samples such that long time-scale, low-energy electron microscopy can be used for high-resolution imaging of MoS<sub>2</sub>. In addition, our results show that potassium deposition enables enhancement of the imaging of surface structure down to  $\sim 0.5 \mu\text{m}$  size. This appears to be due to preferential nucleation of potassium at defect sites, as supported below in our measurements of potassium-dosed CVD-grown MoS<sub>2</sub>. More generally, this procedure serves as a useful method to enhance the imaging and diagnostic capability of LEEM.

### 3. LEED on Si-supported exfoliated MoS<sub>2</sub>

The crystal quality and orientation of our 2D materials were probed in reciprocal space using  $\mu$ -LEED. Initial experimentation showed that an atomically flat, single-domain

crystal flake with an area of  $> 10 \times 10 \mu\text{m}^2$  was needed to obtain a sharp LEED pattern. Using samples that conformed to these criteria, LEED measurements were performed on “stand-alone” 1–4 ML islands, along with a thin bulk MoS<sub>2</sub> flake, shown in Figs. 1(h)–1(k). Note that for a MoS<sub>2</sub> sample with a layer thickness greater than 1 ML, the LEED pattern was almost as sharp as that from bulk MoS<sub>2</sub>. The mean free path for 48 eV electrons, used in Fig. 1, is  $\sim 5.17 \text{ \AA}$  [47,48], which is comparable to the thickness of 1 ML MoS<sub>2</sub>; this suggests that LEED spot broadening observed for 1 ML MoS<sub>2</sub> Fig. 1(h) is, in part, due to scattering from the substrate. With increasing MoS<sub>2</sub> thickness, this scattering contribution would be expected to decrease, as is indeed shown in Figs. 1(i)–1(k). Our observations of the width of the specular (00) LEED spot support this assertion and show that background scattering from the substrate is diminished for > 2 ML MoS<sub>2</sub>. Spot-width broadening may also be due to substrate-induced roughness, in which the corrugation of the MoS<sub>2</sub> conforms to the corrugation of the underlying substrate, as is the case in monolayer graphene [39]. However, monolayer MoS<sub>2</sub> is much thicker (three atomic layers) than graphene (one atomic layer) and is expected to be much more rigid; the elastic bending modulus

of MoS<sub>2</sub> is calculated to be 9.61 eV, which is much larger than that of graphene, i.e., 1.4 eV [49]. Thus, we expect the effect of substrate-induced roughness to be less in ML MoS<sub>2</sub> compared to graphene, though we cannot completely rule it out. While beyond the scope of this paper, we note that an electron-energy-dependent LEED spot-width analysis, which takes into account the different contributions from Mo and S atoms, could provide important information regarding corrugation in monolayer and multilayer MoS<sub>2</sub> [39,50].

To summarize, our surface-sensitive reciprocal-space measurements reveal single-crystal MoS<sub>2</sub> after transfer, which complements and verifies the above real-space LEEM measurements. Analysis of the width of the (00) spot reveals a monotonic decrease with thickness, which is attributed to a decrease in the scattering of low-energy electrons by the underlying SiO<sub>2</sub>/Si substrate.

### B. Experiments on CVD-grown MoS<sub>2</sub>

The procedures required for successful LEEM imaging of exfoliated MoS<sub>2</sub>, discussed above, allowed us to carry out LEEM measurements on CVD MoS<sub>2</sub> islands grown on SiO<sub>2</sub> substrates. The growth of CVD MoS<sub>2</sub> on SiO<sub>2</sub> has recently been shown to result in the growth of 2D islands with a well-defined set of shapes. One particularly distinctive and prevalent geometry is a ML-thick triangle, with two different types of edge termination [21]; another frequently observed shape is

that of a ML hexagram [Figs. 2(a)–2(c)]. The triangular-shaped MoS<sub>2</sub> islands are single-domain crystals [21] and exhibit only a slight deformation at the center and at the edge. The six-point star-shaped islands, on the other hand, exhibit centrosymmetric, cyclic, mirror-twin boundaries, based on dark-field (DF) TEM measurements [21].

#### 1. LEEM on SiO<sub>2</sub>-supported CVD MoS<sub>2</sub>

Our growth process did not use any form of seeded or nucleated growth. Instead, the best growth condition was obtained with fully cleaned SiO<sub>2</sub> substrates. The average MoS<sub>2</sub> island size ranged from 1 to 100  $\mu\text{m}$  and was predominantly monolayer MoS<sub>2</sub>. Most islands were uniformly 1 ML in thickness, except for a few islands that exhibited a bilayer or multilayer hexagon patch located in their center region. When present, this patch was no larger than about one-tenth of the island's dimension. MEM images of CVD MoS<sub>2</sub> on SiO<sub>2</sub> are shown in Figs. 2(a) and 2(d). In Fig. 2(d), a large MoS<sub>2</sub> star ( $\sim 50 \mu\text{m}$  from side to side) is in contact with a 10- $\mu\text{m}$ -wide Au grid, with a line spacing of 22.5  $\mu\text{m}$ . As was the case in our experiments on exfoliated MoS<sub>2</sub> on SiO<sub>2</sub>, charging effects persisted even in the presence of a metal grid, with LEEM images becoming blurred, especially near island and contact edges during extended electron exposure.

Potassium deposition, though ineffective in eliminating charging, was found to enhance the imaging of surface

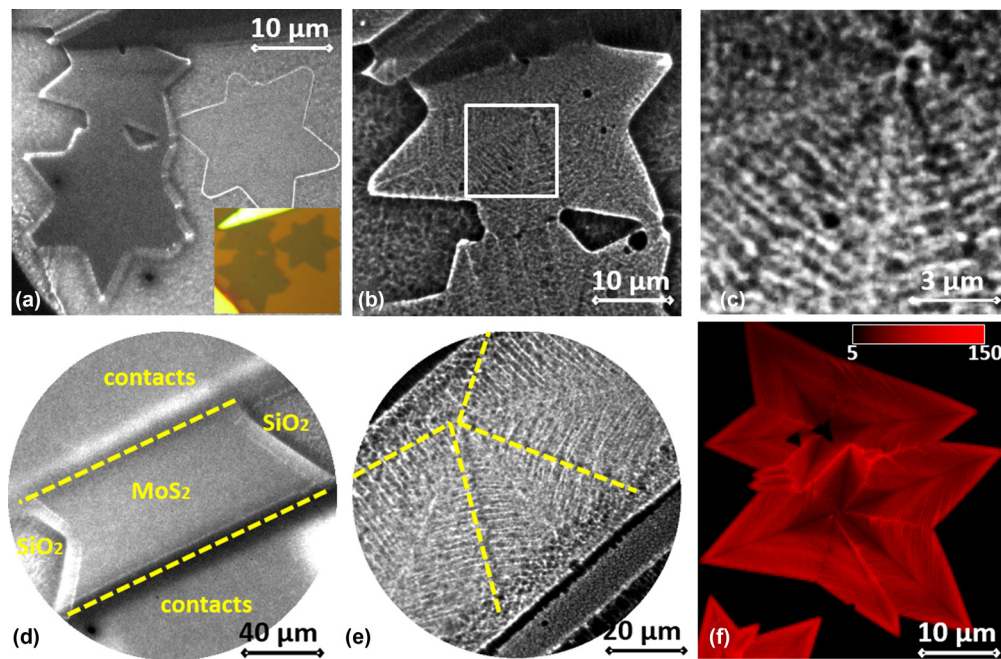


FIG. 2. (Color online) CVD MoS<sub>2</sub> on SiO<sub>2</sub>. (a), (d) LEEM image of multidomain MoS<sub>2</sub> stars on SiO<sub>2</sub>. In (a), two stars to the left were grounded by Au/Cr/Al contacts, as shown in the optical microscopy inset. As can be seen, however, the persistent onset of charging quickly leads to blurring of the LEEM images. The star to the right, which has no connection to the contacts, i.e., is not grounded, shows almost no contrast difference (except for its perimeter) compared to the SiO<sub>2</sub> background. (b), (e) LEEM images after potassium deposition. Potassium deposition enhances the conductivity of the gold-contacted MoS<sub>2</sub> and lowers its work function. It also enhances the contrast of the MoS<sub>2</sub> islands and their sulfur-terminated grain boundaries, revealing a vein-like structure that extends out to the grain boundaries. The yellow dashed lines indicate the grain boundaries that separate crystalline domains. (c) Zoomed-in LEEM image of the selected area in (b). (f) Photoluminescence mapping of an asymmetric multidomain CVD MoS<sub>2</sub> island of comparable size to that of the star in (d) (no potassium doping). This shows that the vein-like structure is not due to potassium doping but is rather a unique feature of CVD MoS<sub>2</sub> grown on SiO<sub>2</sub>. The electron energies used in LEEM are (a)–(c) 0.84 eV and (d)–(e) 0.06 eV.

corrugation. Potassium was deposited until the change in the work function of MoS<sub>2</sub> had saturated with respect to that of the insulating SiO<sub>2</sub> background, as monitored dynamically by MEM. Figure 2(b) shows a LEEM image of a star-shaped island after potassium deposition. The dark dots as marked out in Fig. 2(b) on the MoS<sub>2</sub> island are due to residue originating from the CVD process and can be removed via annealing, as was confirmed by LEEM. One of the most interesting aspects of this figure is that it reveals fine leaf-vein-like topography patterns; a more detailed image of this pattern is shown in Figs. 2(c) and 2(e). To confirm that the leaf-like structure was intrinsic to the MoS<sub>2</sub> instead of being derived from potassium nucleation or intercalation, the amount of potassium deposited was varied; it was then found that the pattern persisted. However, after annealing the sample for two hours at 300 °C to remove potassium, the pattern was no longer visible. By increasing the doping level, the contrast between peaks and valleys of the leaf-like topography pattern increased, although the underlying pattern remained unchanged. This result shows clearly that the deposited potassium enhanced the contrast of our LEEM measurements for the SiO<sub>2</sub>-supported samples. To further confirm this intrinsic vein-like microstructure in CVD MoS<sub>2</sub>, we performed photoluminescence (PL) mapping on a MoS<sub>2</sub> flake of the same origin but without any doping. The result is shown in Fig. 2(f). The spatial variations of the PL intensity are consistent with the microstructure observed by LEEM on potassium-doped samples. One plausible explanation for this phenomenon is that the leaf-like pattern is formed from surface strain built up during the CVD process. Surface strain is known [21,22,39] to create pentagon- and heptagon-shaped MoS<sub>2</sub> microstructures that are derived from hexagon MoS<sub>2</sub> by sulfur-site substitutions at one of the sharing

Mo sites; this microstructure, with alternating 5- or 7-fold MoS<sub>2</sub> rings, corresponds to the recently reported Mo-oriented dislocation found in Ref. [22]. Moreover, surface strain can also create an 8-4-4 type of fold of MoS<sub>2</sub> rings, as reported in Ref. [21].

Thus, in summary, our LEEM observations show by direct imaging that the star-shaped crystals are multidomain crystals, with crystal grain boundaries that can be resolved through potassium dosing. Though we did not perform DF LEEM measurements here, we note that corresponding DF-TEM results can be found in Ref. [21]. This potassium doping also reveals vein-like surface structures, which are attributed to growth-induced strain. This observation reconciles photoluminescence measurements, which show similar nanostructures, albeit with lower resolution.

**2. LEEM on Si-supported CVD MoS<sub>2</sub>**

As mentioned above, optimal electron-probe measurements required transfer of CVD-grown MoS<sub>2</sub> islands from the SiO<sub>2</sub>/Si substrate to a native-oxide-covered Si substrate. Details of the transfer process for CVD MoS<sub>2</sub> can be found in the supplemental materials [36]; after transfer, MoS<sub>2</sub>/Si samples were annealed at 350 °C for 12 hours under UHV prior to measurements. Figure 3 shows LEEM measurements of the transferred MoS<sub>2</sub> islands; these measurements examined the structure and quality of the transferred CVD MoS<sub>2</sub> crystals. In Figs. 3(a) and 3(d), LEEM images of transferred MoS<sub>2</sub> stars and triangles show that the transfer process was successful in preserving the structures originally grown prior to the transfer step. Fractures or cracks, however, were observed along the domain boundaries of star-shaped and other multidomain

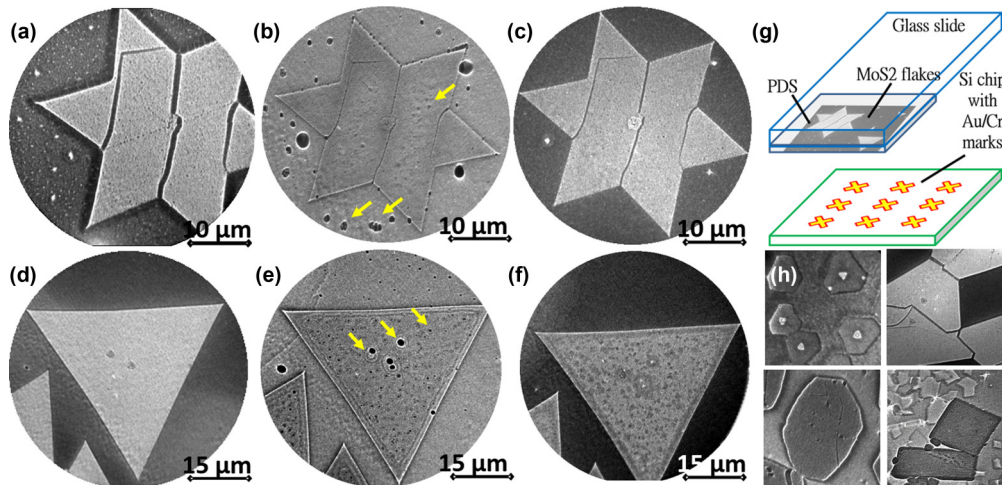


FIG. 3. (Color online) CVD MoS<sub>2</sub> on Si. (a), (d) LEEM images of selected islands with star and triangular shapes, respectively. Sharp edges indicate they are Mo-terminated [21]. In (a), the dark lines are the cracks along the domain boundaries after the transfer process. (b), (e) LEEM images showing the islands after the first potassium doping cycle (see text); note that the reflectivity of the background Si substrate was raised by doping, indicating a lowered work function. Potassium nucleation (marked by the yellow arrows) forms on the surface upon potassium deposition. The density of these islands increases with potassium deposition. (c), (f) LEEM images taken after potassium was removed from the surface via annealing at 160 °C for 1.5 hour and then at 350 °C for 15 min. This annealing reduces the density of the potassium islands and returns the work function to its original level prior to potassium deposition. (g) A sketch illustrating how the CVD MoS<sub>2</sub> adhered on a polydioxanone (PDS) layer was transferred onto a prepatterned Si chip. (h) LEEM images with examples of polycrystalline MoS<sub>2</sub> aggregates of different orientations obtained under different growth conditions. In this particular case, differently oriented domains of MoS<sub>2</sub> islands intersected during CVD growth and exhibited fracturing along their faceted tilt grain boundaries after sample transfer. The electron energies used in LEEM are (a) 0.9 eV, (b) 1.9 eV, (c) 1 eV, (d) 0.54 eV, (e) 2.1 eV, (f) 1 eV, and (h) 0.58 eV.

MoS<sub>2</sub> islands, as shown in Figs. 3(a) and 3(h). Given that these cracks are not seen in the pretransferred CVD samples, it is assumed that the force exerted during the stamping step of the transfer process led to the fracturing. In contrast, triangle-shaped islands did not display any fracturing, which may be explained by their single-domain nature, as confirmed by previously reported TEM measurements performed using MoS<sub>2</sub> on TEM support grids [21]. Besides the multidomain nature of some of the grown crystals,  $\mu$ -LEED measurements of exfoliated and CVD-grown MoS<sub>2</sub> were found to show comparable crystallinity, indicating they are of similar quality. The  $\mu$ -LEED measurements are discussed in detail below.

Given the value of using potassium deposition to enhance topographic features in SiO<sub>2</sub>-supported CVD MoS<sub>2</sub>, this same approach was used to investigate the possible presence of fine topographic features in Si-supported CVD MoS<sub>2</sub> crystals. As in the exfoliated case, potassium dosing led to a 1.75 eV reduction of the MoS<sub>2</sub> work function. Unlike the case of SiO<sub>2</sub>-supported CVD MoS<sub>2</sub> (see Fig. 2), however, LEEM measurements on transferred MoS<sub>2</sub> stars revealed a smooth and vein-free topography, as verified under different doses of potassium. As shown in Figs. 3(d)–3(f), LEEM measurements taken after doping with a dose equivalent to that used in Figs. 2(b) and 2(e) revealed no fine vein structure. The absence of the vein structure is attributed to a release of growth-induced crystal strain during sample transfer. On the other hand, it was observed that potassium deposition did in some cases lead to submicron nucleation on both MoS<sub>2</sub> islands and the Si substrate, at sites of surface structural impurities. At room temperature and under UHV conditions, it has been shown that adsorbed potassium does not intercalate with bulk MoS<sub>2</sub> [51], unlike the case of Cs on bulk MoS<sub>2</sub> [52], and that adsorbed potassium can be removed from the surface by annealing, which occurs at a temperature-dependent desorbing rate [51]. It was also found that adsorbed potassium forms 2D islands on bulk MoS<sub>2</sub> at low coverage and that coverage can be calibrated using changes in the work function [51]. In the present case of ML MoS<sub>2</sub>, these potassium features nucleated preferentially around defects and/or impurities at low coverage; furthermore, we observed that the density of these nucleation increased with potassium dose.

Having investigated the effects of potassium deposition, as described above, we investigated the ability to desorb it by subjecting the sample to different annealing treatments. While annealing at 100–120 °C for 70 minutes did not produce a significant change, subsequent annealing of the sample at 150 °C for 30 minutes decreased the density of potassium nucleation, as shown in Figs. 3(c) and 3(f). In addition, LEEM measurements of a star-shaped MoS<sub>2</sub> island after annealing revealed a clean crystal with well-defined edges, while in the case of a triangle-shaped MoS<sub>2</sub> island, additional annealing at 350 °C for 12 hours was used to obtain a cleaner triangle-shaped MoS<sub>2</sub> island, with little to no evidence of potassium. Thus, potassium deposition appears to be a nondestructive and reversible technique for enhancing the study of monolayer MoS<sub>2</sub> using electron-probe-based instruments.

To summarize our observations in this section, LEEM measurements enable examination of the 0.5- $\mu$ m-scale structure of transferred CVD-grown MoS<sub>2</sub>. In addition, these measurements revealed occasional fracturing of multidomain crystals,

which was observed to occur along grain boundaries. In contrast to as-grown CVD MoS<sub>2</sub> supported by thick SiO<sub>2</sub>/Si, transferred CVD MoS<sub>2</sub> does not exhibit a vein-like surface structure, which suggests that growth-induced strain is released upon transfer. As in the above cases, potassium deposition is a useful diagnostic technique in enhancing contrast because it preferentially nucleates at impurity and defect sites, and as shown in this section, it is also nondestructive and reversible.

### 3. LEED on CVD MoS<sub>2</sub>

The crystalline structure of CVD MoS<sub>2</sub> was investigated using  $\mu$ -LEED measurements on our two types of substrates, as shown in Fig. 4. As  $\mu$ -LEED is sensitive to crystal deformation on length scales from  $\sim$ 20 nm to interatomic distances, it complements real-space images by providing additional information about surface deformation at very short length scales, i.e.,  $\sim$ 10 nm or less. Figures 4(a)–4(c) shows measurements on one domain of an electrically contacted multidomain star-shaped CVD-grown crystal. LEED measurements alternated between 3-fold and 6-fold symmetric patterns with increasing electron energies [53]. The alternation between 3- and 6-fold diffraction symmetry corresponds to the LEED beam probing more than the top atomic layer. A complete explanation, however, would require application of LEED multiscattering theory over the electron probing depth, which is beyond the scope of this paper.

As shown in Figs. 4(d)–4(f), LEED patterns taken from transferred CVD MoS<sub>2</sub> are identical to those from nontransferred CVD MoS<sub>2</sub> on SiO<sub>2</sub>, except for a broadening of the spot widths. In the case of exfoliated MoS<sub>2</sub>, a similar broadening is present after transfer to a Si substrate. In order to determine if this broadening is intrinsic to MoS<sub>2</sub> rather than extrinsic in nature, we undertook the following analysis. First, we analyzed the widths of the first-order diffraction spots, since these spots are derived solely from MoS<sub>2</sub> and thus minimize any possible spot-width broadening originating from the underlying substrate, which would appear in the (00) spot. Second, we analyzed the spot widths not only for the case of a transferred exfoliated substrate-supported MoS<sub>2</sub>, but also for a transferred exfoliated *suspended* MoS<sub>2</sub>. In this case, the MoS<sub>2</sub> is supported above a well, etched [39] in the Si, as shown in Fig. 4(g). We find similar spot widths for the supported and the suspended cases, which leads us to attribute the spot width broadening post-transfer to primarily intrinsic factors. Although the exact origin of this spot broadening is unknown at this time, given that it is apparently intrinsic to transferred MoS<sub>2</sub>, per the above observations, it appears to be rooted in the transfer process.

Figures 4(g)–(4i) shows the exfoliated, transferred-to-Si, 1 ML, single-crystal MoS<sub>2</sub>, which served as a reference for comparison with transferred-to-Si, CVD MoS<sub>2</sub>. The LEED spot width is comparable for both the transferred exfoliated and the transferred CVD MoS<sub>2</sub>, indicating that the sample quality of CVD MoS<sub>2</sub> islands, including surface quality and crystallinity, is comparable to exfoliated crystals. To better support this statement, a comparison of the full-width at half-maximum (FWHM) of the LEED (00) spot and first-order diffraction spots, as determined by Gaussian fitting after intensity normalization and detector background-signal removal, was performed. An example of this fitting is shown in Fig. 4(j),

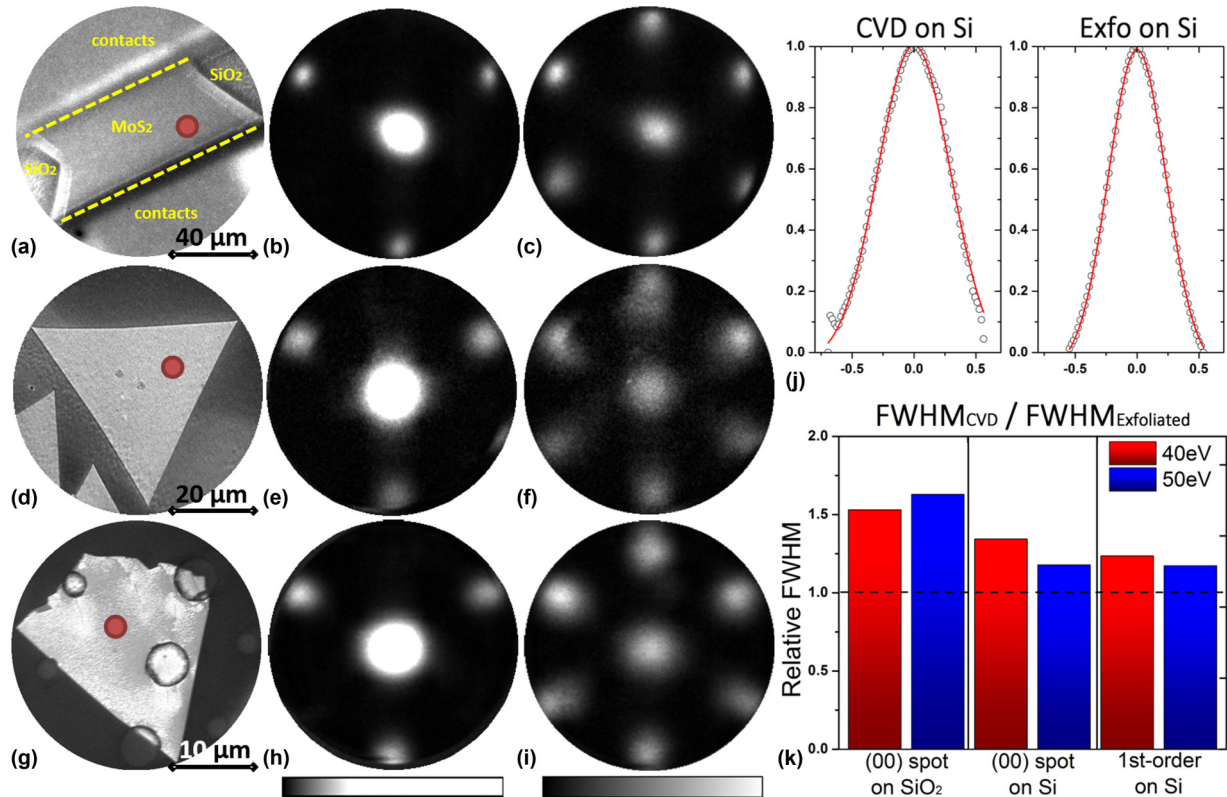


FIG. 4. (Color online) Comparison of 1 ML MoS<sub>2</sub> using  $\mu$ -LEED. (a)–(c) CVD MoS<sub>2</sub> on SiO<sub>2</sub>, (d)–(f) CVD MoS<sub>2</sub> transferred onto native-oxide terminated silicon, (g)–(i) CVD MoS<sub>2</sub> exfoliated and transferred onto native-oxide terminated silicon. (a), (d), (g) LEEM images at energy 0.06 eV, 0.46 eV, and 5 eV, respectively. The red circle denotes the location of the  $\mu$ -LEED measurement spot, having a diameter of 2  $\mu$ m. (b), (e), (h) LEED patterns at 40 eV electron energy. (c), (f), (i) LEED at 50 eV. The LEED pattern shows transitions between 3- and 6-fold symmetry at different electron energies. Also, the (00) LEED spot widths for (d) and (g) are comparable. (j) Normalized-intensity line profile of the (00) LEED spot of CVD and exfoliated MoS<sub>2</sub> on Si; horizontal axis units are  $\text{\AA}^{-1}$ . (k) Comparison between pretransferred MoS<sub>2</sub> on SiO<sub>2</sub> and post-transferred MoS<sub>2</sub> on Si for two different energies. The relative FWHM values are derived from the (00) and the first-order spots of the CVD MoS<sub>2</sub> divided by that of exfoliated MoS<sub>2</sub> on the same substrate.

and a comparison of the FWHM of CVD and exfoliated MoS<sub>2</sub> at two different electron energies is shown in Fig. 4(k). Before transfer, the CVD-grown MoS<sub>2</sub> has a larger FWHM relative to the pretransferred exfoliated MoS<sub>2</sub>, which corresponds to a rougher surface and is presumably due to the strain-induced wrinkles as shown in Fig. 2. Upon transfer to a Si substrate, however, the strain-induced vein-like wrinkles are no longer present, as noted above, and hence result in a comparable FWHM between transferred CVD and transferred exfoliated MoS<sub>2</sub>. This supports our real-space LEEM measurements in which CVD-grown MoS<sub>2</sub> appeared quite similar in quality to exfoliated MoS<sub>2</sub>. Thus, our  $\mu$ -LEED measurements confirmed the structural integrity of as-grown CVD and transferred CVD MoS<sub>2</sub> and enabled the determination of the crystal domain orientations. More importantly, these  $\mu$ -LEED measurements show that CVD-grown MoS<sub>2</sub> is of comparable quality to exfoliated MoS<sub>2</sub>.

#### IV. CONCLUSION

In this work, the surface morphology and structural quality of ultrathin MoS<sub>2</sub> flakes originating from mechanical exfoliation and CVD growth were examined and compared using LEEM and  $\mu$ -LEED. A major experimental issue for our measurements was sample charging and surface corrugation.

The charging was eliminated by transferring MoS<sub>2</sub> crystals to a native-oxide-covered Si wafer, a procedure which was compatible with our LEEM and LEED measurements. In addition, surface doping techniques by an alkali metal were crucial for these MoS<sub>2</sub> studies. These electron-probe measurements enabled detailed surface structural characterization and added complementary insight to those obtained earlier from Raman and PL measurements [7,12]. In particular, real-space probing by LEEM in conjunction with  $k$ -space probing by  $\mu$ -LEED shows that CVD-grown MoS<sub>2</sub> single crystals have comparable crystal quality to that of exfoliated MoS<sub>2</sub>. In addition, our results have also shown that as-grown CVD MoS<sub>2</sub> sample islands have a fine vein-like or rippled structure, as revealed via potassium deposition; this leaf-like morphology is lost after sample transfer to a silicon substrate. We attribute this structure to strain fields formed during CVD growth. Our observations reported here are an important step toward a broader understanding of MoS<sub>2</sub> surface morphology on different substrates and establishing strategies for MoS<sub>2</sub> synthesis.

#### ACKNOWLEDGMENTS

The beamline measurements and analyses and the sample preparation were funded by the AFOSR MURI Program on

new graphene materials science and technology, Grant No. FA9550-09-1-0705, and were carried out in part at the Center for Functional Nanomaterials and National Synchrotron Light Source, Brookhaven National Laboratory, which is supported by the US Department of Energy (USDOE), Office of Science, Basic Energy Sciences, under Contract No. DE-AC02-98CH10886. The sample growth and transfer work

and optical examination (by D.Z., A.M.Z., D.C., I.P.H., and J.H.) were supported as part of the Center for Redefining Photovoltaic Efficiency through Molecular Scale Control, an Energy Frontier Research Center funded by the USDOE, Office of Science, Basic Energy Sciences, under Award No. DE-SC0001085. We thank the anonymous referee for the excellent suggestions that helped improve this paper.

- [1] K. S. Novoselov, *Rev. Mod. Phys.* **83**, 837 (2011).
- [2] K. F. Mak, K. He, C. Lee, G. H. Lee, J. Hone, T. F. Heinz, and J. Shan, *Nat. Mater.* **12**, 207 (2013).
- [3] J. S. Ross, S. Wu, H. Yu, N. J. Ghimire, A. M. Jones, G. Aivazian, J. Yan, D. G. Mandrus, D. Xiao, W. Yao, and X. Xu, *Nat Commun.* **4**, 1474 (2013).
- [4] T. Cheiwchanchamnangij and W. R. L. Lambrecht, *Phys. Rev. B* **85**, 205302 (2012).
- [5] A. Ramasubramaniam, *Phys. Rev. B* **86**, 115409 (2012).
- [6] W. Jin, P.-C. Yeh, N. Zaki, D. Zhang, J. T. Sadowski, A. Al-Mahboob, A. M. van der Zande, D. A. Chenet, J. I. Dadap, I. P. Herman, P. Sutter, J. Hone, and R. M. Osgood, Jr., *Phys. Rev. Lett.* **111**, 106801 (2013).
- [7] A. Splendiani, L. Sun, Y. Zhang, T. Li, J. Kim, C.-Y. Chim, G. Galli, and F. Wang, *Nano Lett.* **10**, 1271 (2010).
- [8] K. F. Mak, K. He, J. Shan, and T. F. Heinz, *Nature Nanotech.* **7**, 494 (2012).
- [9] H. Zeng, J. Dai, W. Yao, D. Xiao, and X. Cui, *Nature Nanotech.* **7**, 490 (2012).
- [10] T. Cao, G. Wang, W. Han, H. Ye, C. Zhu, J. Shi, Q. Niu, P. Tan, E. Wang, B. Liu, and J. Feng, *Nature Commun.* **3**, 887 (2012).
- [11] Y. Li, Y. Rao, K. F. Mak, Y. M. You, S. Wang, C. R. Dean, and T. F. Heinz, *Nano Lett.* **13**, 3329 (2013).
- [12] K. F. Mak, C. Lee, J. Hone, J. Shan, and T. F. Heinz, *Phys. Rev. Lett.* **105**, 136805 (2010).
- [13] O. Brontvein, D. G. Stroppa, R. Popovitz-Biro, A. Albu-Yaron, M. Levy, D. Feuerman, L. Houben, R. Tenne, and J. M. Gordon, *J. Am. Chem. Soc.* **134**, 16379 (2012).
- [14] Y. Li, H. Wang, L. Xie, Y. Liang, G. Hong, and H. Dai, *J. Am. Chem. Soc.* **133**, 7296 (2011).
- [15] G. Eda, H. Yamaguchi, D. Voiry, T. Fujita, M. Chen, and M. Chhowalla, *Nano Lett.* **11**, 5111 (2011).
- [16] A. R. Botello-Mendez, F. López-Urías, M. Terrones, and H. Terrones, *Nanotechnology* **20**, 325703 (2009).
- [17] Y.-H. Lee, X.-Q. Zhang, W. Zhang, M.-T. Chang, C.-T. Lin, K.-D. Chang, Y.-C. Yu, J. T.-W. Wang, C.-S. Chang, L.-J. Li, and T.-W. Lin, *Adv. Mater.* **24**, 2320 (2012).
- [18] Y. Zhan, Z. Liu, S. Najmaei, P. M. Ajayan, and J. Lou, *Small* **8**, 966 (2012).
- [19] K.-K. Liu, W. Zhang, Y.-H. Lee, Y.-C. Lin, M.-T. Cheng, C.-Y. Su, C.-S. Cheng, H. Li, Y. Shi, H. Zhang, C.-S. Lai, and L.-J. Li, *Nano Lett.* **12**, 1538 (2012).
- [20] Y. Shi, W. Zhou, A.-Y. Lu, W. Fang, Y.-H. Lee, A. L. Hsu, S. M. Kim, H. Y. Yang, L.-J. Li, J.-C. Idrobo, and J. Kong, *Nano Lett.* **12**, 2784 (2012).
- [21] A. M. van der Zande, P. Y. Huang, D. A. Chenet, T. C. Berkelbach, Y. M. You, G.-H. Lee, T. F. Heinz, D. R. Reichman, D. A. Muller, and J. C. Hone, *Nature Mater.* **12**, 554 (2013).
- [22] S. Najmaei, Z. Liu, W. Zhou, X. Zou, G. Shi, S. Lei, B. I. Yakobson, J. C. Idrobo, P. M. Ajayan, and J. Lou, *Nature Mater.* **12**, 754 (2013).
- [23] B. Radisavljevic, A. Radenovic, J. Brivio, V. Giacometti, and A. Kis, *Nature Nanotech.* **6**, 147 (2011).
- [24] C. R. Dean, A. F. Young, I. Meric, C. Lee, L. Wang, S. Sorgenfrei, K. Watanabe, T. Taniguchi, P. Kim, K. L. Shepard, and J. Hone, *Nature Nanotech.* **5**, 722 (2010).
- [25] L. Britnell, R. V. Gorbachev, A. K. Geim, L. A. Ponomarenko, A. Mishchenko, M. T. Greenaway, T. M. Fromhold, K. S. Novoselov, and L. Eaves, *Science* **24**, 947 (2012).
- [26] Z. Yin, H. Li, H. Li, L. Jiang, Y. Shi, Y. Sun, G. Lu, Q. Zhang, X. Chen, and H. Zhang, *ACS Nano* **6**, 74 (2012).
- [27] M. Fontana, T. Deppe, A. Boyd, M. Rinzan, A. Liu, M. Paranjape, and P. Barbara, *Sci. Rep.* **3**, 1634 (2013).
- [28] T. H. Schmidt, S. Heun, J. Slezak, J. Diaz, K. C. Prince, G. Lilienkamp, and E. Bauer, *Surf. Rev. Lett.* **05**, 1287 (1998).
- [29] E. Bauer, *Rep. Prog. Phys.* **57**, 895 (1994).
- [30] J. I. Flege, E. Vescovo, G. Nintzel, L. H. Lewis, S. Hulbert, and P. Sutter, *Nucl. Instrum. Meth. B* **261**, 855 (2007).
- [31] P. Sutter and E. Sutter, *Adv. Func. Mat.* **23**, 2617 (2013).
- [32] T. Ohta, A. Bostwick, T. Seyller, K. Horn, and E. Rotenberg, *Science* **313**, 951 (2006).
- [33] J.-H. Chen, C. Jang, S. Adam, M. S. Fuhrer, E. D. Williams, and M. Ishigami, *Nature Physics* **4**, 377 (2008).
- [34] M. S. Choi, G.-H. Lee, Y.-J. Yu, D.-Y. Lee, S. H. Lee, P. Kim, J. Hone, and W. J. Yoo, *Nature Commun.* **4**, 1624 (2013).
- [35] L. Britnell, R. M. Ribeiro, A. Eckmann, R. Jalil, B. D. Belle, A. Mishchenko, Y.-J. Kim, R. V. Gorbachev, T. Georgiou, S. V. Morozov, A. N. Grigorenko, A. K. Geim, C. Casiraghi, A. H. Castro Neto, and K. S. Novoselov, *Science* **340**, 1311 (2013).
- [36] See Supplemental Material at <http://link.aps.org/supplemental/10.1103/PhysRevB.89.155408> for sample preparation session, for wet transfer process via PMMA/PVA layer for exfoliated MoS<sub>2</sub>, and dry transfer process via PDS for CVD MoS<sub>2</sub>.
- [37] K. S. Novoselov, D. Jiang, F. Schedin, T. J. Booth, V. V. Khotkevich, S. V. Morozov, and A. K. Geim, *Proc. Natl. Acad. Sci. USA* **102**, 10451 (2005).
- [38] A. Ayari, E. Cobas, O. Ogundadegbe, and M. S. Fuhrer, *J. Appl. Phys.* **101**, 014507 (2007).
- [39] A. Locatelli, K. R. Knox, D. Cvetko, T. O. Menten, M. A. Nino, S. Wang, B. Y. Mehmet, P. Kim, R. M. Osgood, Jr., and A. Morgante, *ACS Nano* **4**, 4879 (2010).
- [40] J. T. Sadowski, *Opt. Mater.* **34**, 1635 (2012).
- [41] R. Godehardt, *Adv. Imag. Electr. Phys.* **94**, 81 (1995).
- [42] O. H. Griffith, K. K. Hedberg, D. Desloge, and G. F. Rempfer, *J. Microsc.* **168**, 249 (1992).
- [43] A. E. Luk'yanov, G. V. Spivak, and R. S. Gvozdover, *Sov. Phys.-Usp.* **16**, 529 (1974).
- [44] See Supplemental Material at <http://link.aps.org/supplemental/10.1103/PhysRevB.89.155408> for potassium deposition session, for MEM imaging mode in LEEM, and surface potential monitoring.

- [45] M. M. Benameur, B. Radisavljevic, J. S. Héron, S. Sahoo, H. Berger, and A. Kis, *Nanotechnology* **22**, 125706 (2011).
- [46] M. A. van Hove, S. Y. Tong, and M. H. Elconin, *Surface Sci.* **64**, 85 (1977).
- [47] M. P. Seah and W. A. Dench, *Surf. Interface Anal.* **1**, 2 (1979).
- [48] By using the mean free path formula for compounds in Ref. [47] and the thickness of  $\text{MoS}_2 = 0.72$  nm from Ref. [16], we calculate a  $\sim 5.2$  Å mean-free-path for ML  $\text{MoS}_2$ .
- [49] J. W. Jiang, Z. Qi, H. S. Park, and T. Rabczuk, *Nanotechnology* **24**, 435705 (2013).
- [50] R. M. Feenstra, N. Srivastava, Q. Gao, M. Widom, B. Diaconescu, T. Ohta, G. L. Kellogg, J. T. Robinson, and I. V. Vlassiuk, *Phys. Rev. B* **87**, 041406 (2013).
- [51] C. A. Papageorgopoulos, M. Kamaratos, S. Kennou, and D. Vlachos, *Surf. Sci.* **251-252**, 1057 (1991).
- [52] S. Kennou, S. Ladas, and C. Papageorgopoulos, *Surf. Sci.* **152-153**, 1213 (1985).
- [53] F. Jona, J. A. Strozier, Jr., and W. S. Yang, *Rep. Prog. Phys.* **45**, 527 (1982).